

# Ray chaos and $Q$ -spoiling in Lasing Droplets

A. Mekis, J. U. Nöckel, G. Chen, A. D. Stone and R. K. Chang

*Applied Physics, Yale University, P.O. Box 208284, New Haven, Connecticut 06520-8284*

(Received 26 May 1995)

It is proposed that the spoiling of high  $Q$  whispering gallery modes in deformed dielectric spheres can be understood as a transition to chaotic ray dynamics which can no longer be confined by total internal reflection. This is a KAM/Lazutkin transition for light. The theory is applied to explain the lasing properties of droplets.

PACS numbers: 05.45+b, 42.55.Mv

*Published in Phys. Rev. Lett.* **75**, 2682 (1995)

The highest  $Q$  optical resonators known are dielectric microspheres in which the high  $Q$  modes are created by total internal reflection of light circulating just inside the surface of the sphere [1, 2]. These high  $Q$  modes are referred to as “whispering gallery” (WG) modes or alternatively as “morphology-dependent resonances” (MDR’s) [2]. If the dielectric is a liquid droplet containing an appropriate dye then the droplet acts as a high  $Q$  micro-resonator to support lasing action of the dye when optically pumped [3]. The resonance properties of an ideal spherical dielectric, for which the wave equation separates, are described by Mie theory where the quasi-modes are the product of spherical Bessel functions  $j_l(nkr)$  ( $n$  is the index of refraction) and vector spherical harmonics [4]. The radial equation then contains a repulsive term  $l(l+1)/r^2$  which is the analogue of the angular momentum barrier for light rays and an effectively attractive term associated with the higher index of refraction in the liquid. The combination of the attractive “well” represented by the dielectric and the repulsive angular momentum barrier gives rise to quasi-bound states of the effective potential near the rim of the droplets [4] for certain ratios of  $l$  to  $kR$  ( $k$  is the wavevector in vacuum,  $R$  the radius of the spherical droplet). In the ideal sphere these resonances are only broadened by evanescent leakage (“tunneling”), hence their enormous  $Q$  values.

Because these resonances arise from angular mo-

mentum conservation, deviations of the dielectric from spherical symmetry should ultimately lead to spoiling of these high- $Q$  modes. However perturbative treatments [5] valid for small deformations ( $< .001R$ ) of the sphere just mix nearby modes and do not find a large degradation of their  $Q$ . At larger deformations ( $\geq .01R$ ) many hundreds of modes are mixed and although numerical solution of the wave equation is possible, no qualitative understanding of the  $Q$ -spoiling behavior had been proposed in the literature. Recently several of the authors [6] developed a ray-optics model to describe the physics when  $kR \gg 1$  and the fractional deformation is larger than 1%; and applied it to two-dimensional or cylindrically symmetric dielectrics. The basic idea is that if a ray starting nearly tangent to the interior surface (i.e. in a WG trajectory) can escape refractively after multiple reflections then the  $Q$  of the corresponding modes will be strongly degraded. The onset of this “classical escape” will be precisely the KAM/Lazutkin transition [7, 8] in the ray dynamics; a very fundamental phenomenon in the theory of the transition to chaos in Hamiltonian systems. This phenomenon, which is analogous to a second order phase transition in phase-space [9], has only been measured experimentally in a few contexts (e.g. advection of a passive scalar in fluid mechanics). Hence the  $Q$ -spoiling of these modes will be a signature of the Hamiltonian transition to chaos. In this Letter we apply our ray-optics

model to three-dimensional axially symmetric dielectrics and show how the model can explain naturally the lasing intensity profile of deformed liquid droplets, which was not previously understood. Thus we address (for the first time, to our knowledge) the properties of a laser with a partially chaotic closed resonator.

For a uniform dielectric body the ray dynamics is just the Hamiltonian dynamics of a point mass moving freely within a three-dimensional “billiard” and specularly reflecting from the surface, with the condition that if the angle of incidence with respect to the normal to the surface,  $\chi$ , falls below the critical angle,  $\sin \chi_c = 1/n$ , then the ray escapes the dielectric according to Snell’s law. A WG mode of angular momentum  $l$  in the undeformed sphere can be associated with a particular value of  $\sin \chi$  within the eikonal approximation; one finds [10]  $\sin \chi \approx l/nkR$  (where the lowest mode of a given  $l$  has  $l/kR \approx n$ ). In order to estimate the  $Q$  of this mode within the deformed sphere we propagate a uniform phase space distribution of rays with this value of  $\sin \chi$  forward in time, compute numerically the mean escape rate  $1/\tau$ , and evaluate  $Q = ck\tau$ . The droplets studied are produced with rotational symmetry around the flow direction (z-axis) so we describe their shape in cylindrical coordinates  $(\rho, \phi, z)$  by the equation  $\rho = \rho_b(z)$  (independent of  $\phi$ ).  $\rho_b(z)$  describes volume-preserving convex deformations of a sphere of radius  $R$ ; hence the maximum  $\rho_m = \rho_b(0)$  and  $\rho_b(z)$  is monotonically decreasing until it reaches zero at the “pole” of the droplet (we shall assume  $\rho_b(z) = \rho_b(-z)$  for simplicity). Although deformations which do not generate ray chaos are possible (e.g. ellipsoidal deformations [11]) generic deformations reduce the number of constants of motion by one and lead at least to the formation of chaotic layers in phase-space. Again generically these layers grow and fill all of phase space as the deformation increases; for example we find a simple quadrupolar deformation of roughly 25% of the radius is sufficient. A pure quadrupole is not however an ideal model for highly deformed droplets since a quadrupole

becomes non-convex when the ratio of the long to short axes is larger than 1.42 whereas the deformed droplets are observed to remain convex up to larger deformations. Therefore in this work we study a family of shapes of the form  $r(\theta) = 1 + \epsilon[\cos^2 \theta + (3/2) \cos^4 \theta]$ .  $\epsilon$  parameterizes the size of the deformation which is prolate with the long/short axis ratio equal to  $1 + (5/2)\epsilon$  (the oblate shape is obtained by changing  $\cos \theta \rightarrow \sin \theta$ ).

Because of the axial symmetry,  $L_z$  is conserved in the ray dynamics, hence phase-space motion is four-dimensional and parameterized by the conserved value of  $L_z$ . At zero deformation the total angular momentum  $\mathbf{L}$  is also conserved but as just noted generic smooth deformations will cause a two-dimensional KAM/Lazutkin transition to chaos. This means that rays describing WG modes corresponding to initial  $\sin \chi_0 \approx 1$  will remain trapped indefinitely for small deformations because the unbroken KAM tori will partition phase space into non-communicating regions and prevent initially tangent rays (WG orbits) from reaching the critical value for escape,  $\sin \chi_c$ . The unbroken tori will manifest themselves as caustics in the real-space ray dynamics [8, 6]. Therefore  $Q$  will be infinite within our model (which neglects tunneling) up to a threshold deformation  $\epsilon_c$  at which the last intervening KAM torus breaks. For deformations larger than  $\epsilon_c$ ,  $Q$  will decrease, initially as  $(\epsilon - \epsilon_c)^{-\alpha}$  where  $\alpha \approx 3$  [6]. Numerical solutions of the wave equation for such systems at  $kR \approx 25$  confirm the existence of a Q-spoiling threshold as predicted by this model[12], although detailed quantitative agreement is not expected for such small values of  $kR$  (in our experimental systems  $kR \approx 500$ ).

The droplets studied are produced by a Berglund-Liu vibrating orifice generator which produces a monodispersed stream of ethanol droplets containing Rhodamine B dye[3]. Although far from the orifice the droplets become quite spherical due to surface tension, near the orifice they are highly deformed and oscillate between oblate and

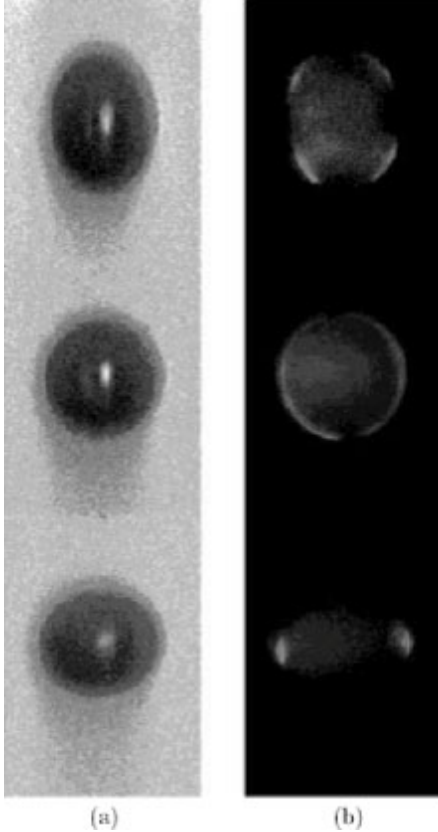


Figure 1: Shadow graphs (a) and simultaneous total-intensity images (b) of three lasing droplets falling in air taken at different phases of oscillation: prolate (top), spherical (middle) and oblate (bottom). Light regions in (b) indicate lasing.

prolate shapes with as much as a factor of two between their long and short axes. These damped oscillations occur on time scales which are long compared to the other relevant time constants of the experiment so droplets of varying deformations can be imaged simply by strobing at the appropriate phase of these oscillations. The basic observations (see Fig. 1) are: 1) Laser emission is always suppressed around the polar regions of the deformed droplets. 2) The region of suppressed lasing is typically much larger for oblate shapes as compared with prolate shapes of the same degree of deformation. 3) In the prolate shapes the equatorial region is more weakly lasing, with the highest lasing intensity coming for arcs centered roughly at  $\pm 45^\circ$  from the equator.

These qualitative features can be explained from an analysis of the non-linear ray dynamics. These dynamics correspond to two degrees of freedom so it is convenient to project the motion onto a 2D cartesian coordinate system with axes  $z, \rho$ . We choose units for which  $E = 1/2, L_z = \rho^2 \dot{\phi}$  and  $\phi(t)$  is completely determined by  $\rho(t)$ . The  $z$  motion is free between collisions with the boundary. The  $\rho$  motion between collisions is determined by energy conservation and the  $L_z$  angular momentum barrier:  $\dot{\rho}^2 = 1 - \dot{z}^2 - L_z^2/\rho^2$ . This means that between each collision  $\rho^2(t)$  describes a parabola with minimum value equal to the classical turning point in the centrifugal potential. For all  $L_z \neq 0$  the rays are repelled from the  $z$ -axis and satisfy the inequality  $\rho(t) \geq L_z$ . Specular reflection of the ray reverses the normal component of the three-dimensional velocity vector; due to the axial symmetry the normal to the droplet has no azimuthal component and thus collisions are specular in the  $z - \rho$  plane as well. Thus the problem is equivalent to a new kind of billiard (which we refer to as a *centrifugal billiard*) with free motion in one direction and the centrifugal force determining motion in the orthogonal direction (see inset, Fig. (2a)).

Since the physical coordinates of most interest to us are the polar angle of each collision  $\tan \theta = \rho/z$  and the 3D Snell angle  $\sin \chi$  (which is simply related to the angle of incidence in the  $z - \rho$  plane) we will plot the Poincaré surfaces of section (SOS) for these billiards using the coordinates  $\theta, \sin \chi$ . Results for  $\epsilon = 0.3$  and decreasing  $L_z$  are shown in Figs. 2(a)-2(d). The empty region of the SOS represent the portion of phase space forbidden by the  $L_z$  barrier. It is easily shown that the boundary of this forbidden region satisfies  $\sin \chi_{min}(\theta) = L_z/\rho_b(\theta)$  implying that the global minimum value of the Snell angle occurs when the ray bounces at the equator and is given by  $\sin \chi_{min} = L_z/\rho_m$ . Thus Q-spoiling by ray escape is completely forbidden by the  $L_z$  angular momentum barrier for  $L_z \geq \rho_m \sin \chi_c$  (Fig. 2a). Since the high  $L_z$  orbits are near the equatorial plane the WG modes corresponding to these orbits will always remain high enough in  $Q$  to

exceed the lasing threshold and the equatorial regions will always provide some degree of laser emission.

However, if  $L_z < \rho_m \sin \chi_c$  and rays are allowed to reach  $\sin \chi_c$  the occurrence of Q-spoiling depends not just on  $L_z$  but on the degree of chaos present in the dynamics. Note that increasing  $L_z$  (for a fixed deformation) not only increases the forbidden regions of the SOS but also decreases the amount of chaos. That is because high  $L_z$  orbits are forced to stay close to the equatorial plane. Orbits in the equatorial plane initially ( $z = 0, \dot{z} = 0$ ) remain there forever and are just the integrable orbits of a circular billiard due to the axial symmetry. Near-equatorial orbits experience a much smaller effective deformation of the droplet than do the near-polar orbits and hence exhibit much less chaos for the same deformation. So classical escape may be allowed by  $L_z$  conservation but forbidden due to the presence of an unbroken torus preventing phase space diffusion to  $\sin \chi_c$  (see Fig 2(b)). For deformations less than roughly 5% this situation holds all the way down to  $L_z = 0$  so that Q remains relatively high for *all* orbits and lasing occurs everywhere on the rim of the droplet. However for deformations greater than 5% the effective non-linearity at sufficiently low  $L_z = L_{zc}$  will be strong enough to break the relevant KAM tori and WG orbits will become chaotic. This means that chaotic regions in the SOS will extend from  $\sin \chi_0$  to  $\sin \chi_c$  and classical Q-spoiling occurs (see Fig. 2c). For all  $L_z < L_{zc}$ , the Q of the associated WG modes will decrease steeply with  $L_z$  and fall below the lasing threshold (see Fig. 3(c)). All orbits of non-zero  $L_z$  are excluded from the polar region and the region of exclusion increases with increasing  $L_z$  (for  $L_z = \rho_m$  the orbit must remain at the equator). Thus if  $L_{zc} \neq 0$  for a given deformation then  $L_{zc}$  determines a minimum allowed value of the polar angle,  $\theta_{min}$ , which divides the high Q modes from the low Q modes [13]. Therefore an arc around the poles of angular size  $\approx 2\theta_{min}$  will not lase for large deformations. This explains why the polar regions of the deformed lasing droplets are dark.

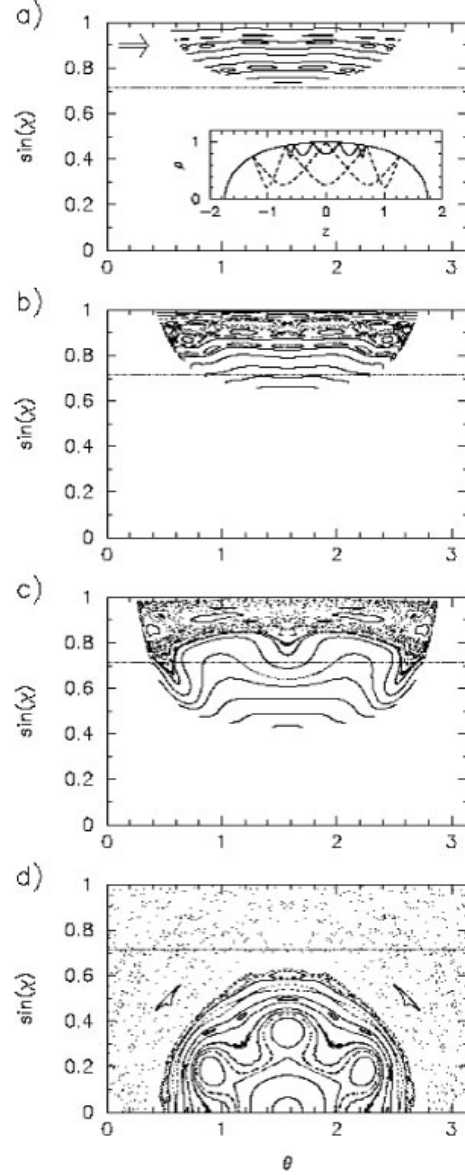


Figure 2: Poincaré surfaces of section for prolate droplets with deformation of  $\epsilon = 0.3$  for  $L_z = 0.735$  (a),  $L_z = 0.65$  (b),  $L_z = 0.43$  (c) and  $L_z = 0$  (d). The arrow to the left indicates the angle of incidence at which the ray bundle is launched,  $\sin \chi_0 \approx 0.9$ , dash-dotted line denotes  $\sin \chi_c = 1/n = .735$  for the droplets of Fig. 1. Inset in (a) shows the droplet shape in the  $z - \rho$  plane and typical trajectories for  $L_z = 0.735$  (solid line) and  $L_z = 0.2$  (dashed line).

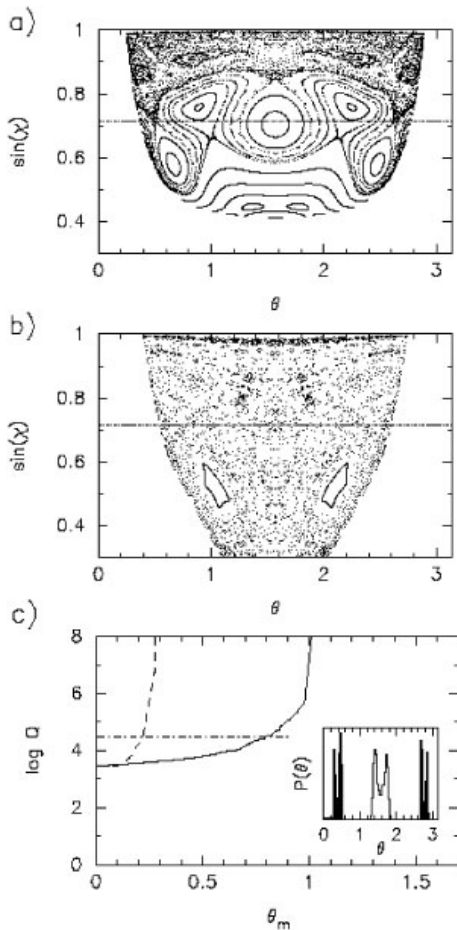


Figure 3: Comparison of prolate (a) versus oblate (b) droplets of the same deformation,  $\epsilon = 0.3$ , and at the same angular momentum,  $L_z = 0.41$ . The arrow and dash-dotted line have the same meaning as in Fig. 2. For the prolate shape, only two thin chaotic channels cross the line at  $\sin \chi_c$ , whereas chaos is fully developed around  $\sin \chi_c$  in the oblate case. Phase-space diffusion is thus expected to lead to faster escape from the oblate droplet. In (c), the resulting  $Q$  factor (assuming  $nkR = 700$ ) is recorded while  $L_z$  is varied. We plot  $Q$  as a function of the minimum polar angle (closest approach to the pole) allowed for the given  $L_z$ , for prolate (dashed) and oblate (solid) shape of  $\epsilon = 0.3$ . Inset to (c) gives the histogram of polar angle at which escape occurs for prolate (dark) and oblate (light) shapes.

The ray-optics model can also explain the observed difference between prolate and oblate droplets. In the prolate droplets the short axis is in the equatorial plane whereas in the oblate droplets it connects the poles. For all smooth convex shapes there is associated with the short axis a stable two-bounce orbit[14] which appears as the island centered on  $\theta = \pi/2$  in the SOS for the prolate shape (Figs. 2(a)-(d), only one island appears because the two bounces occur at  $\theta = \pi/2$ , displaced by  $\pi$  in the azimuthal angle). For the oblate shape this stable orbit connects the poles and for  $L_z = 0$  would be visible as islands at  $\theta = 0, \pi$ ; however this orbit is unreachable due to the  $L_z$  barrier for  $L_z \neq 0$  and is no longer visible in Fig. 3(b). While the short axes are associated with stable islands which provide barriers to phase space diffusion, the long axes are associated with unstable periodic orbits which generate chaos in their vicinity. Hence in the oblate shape this unstable orbit generates chaos in the equatorial region, whereas in the prolate shape it generates chaos in the polar regions *which are typically inaccessible due to the  $L_z$  barrier*. Therefore, for the same ratio of semi-minor to semi-major axes and the same  $L_z$  the oblate shape has more unstable WG orbits and lower  $Q$  associated modes in the polar regions (Figs. 3a-b). Thus just on the basis of their  $Q$  we expect the oblate droplets to have larger dark (non-lasing) regions near the poles than the prolate droplets, as observed. As noted above, once classical ray escape is allowed we can calculate [6] the  $Q$ -value of modes associated with a given  $L_z$  or equivalently a given value of  $\theta_{min}$ ; comparison of  $Q$  vs.  $\theta_{min}$  for the oblate and prolate shapes is shown in Fig. 3c confirming this qualitative reasoning. However Fig. 3c indicates that for reasonable deformations the  $Q$ -values alone do not explain the large difference between the lasing intensity profile of the oblate and prolate droplets (since the  $\theta_{min}$  at which the lasing threshold is crossed only differs by  $30^\circ$ ). Nonetheless Fig. 3c also shows that there is a significant range of  $L_z$  for which  $Q$  exceeds the lasing threshold but classical escape is possible. In this case we expect highly non-uniform emission [6] in the polar angle  $\theta$  since escape will oc-

cur for these modes primarily in the intervals of  $\theta$  where chaos extends down to  $\sin \chi_c$ . These intervals are very different for the prolate and oblate shapes. In Fig. 3a for the prolate shape they are roughly at  $\theta = 45^\circ, 135^\circ$  where the angular momentum boundary intersects  $\sin \chi_c$ , whereas in Fig. 3b for the oblate shape they are centered on the equator. This is the generic behavior over a large range of deformations. Thus for the oblate shape, although emission is allowed up to  $\theta_{min}$ , in fact it occurs over a much narrower angular interval for these modes; whereas in the prolate shape the most intense emission occurs at well-defined polar angles well separated from the equator, which remains relatively dim. An angular intensity profile shown in the inset to Fig. 3c confirms this reasoning for the classically escaping modes above the lasing threshold. Very recent results using the wave equation [12] indicate that even modes which do not escape classically still have an enhanced tunneling probability in the regions where classical escape occurs (because here they approach most closely  $\sin \chi_c$ ). We conjecture that the experimental lasing intensity profile arises from both effects. This issue goes beyond the pure ray-optics model and will require further study.

We thank Dima Shepelyansky for helpful discussions. This work was partially supported by NSF Grant DMR-9215065 and U.S. Army Research Office grants DAAH04-93-G-0009, DAAH04-94-G-0031.

## References

- [1] L.Collot V.Lefevre-Seguin, M.Raimond and S.Haroche, *Europhys.Lett.***23**, 327 (1993).
- [2] S.C.Hill and R.E.Benner, in *Optical Effects Associated with Small Particles*, P.W.Barber and R.K.Chang, Eds. (World Scientific, Singapore 1988).
- [3] S.-X.Qian, J.B.Snow, H.-M.Tzeng, and R.K.Chang, *Science* **231**, 486 (1986).
- [4] B.R.Johnson, *J.Opt.Soc.Am.A* **10**, 343 (1993).
- [5] H.M.Lai, P.T.Leung, K.Young and P.W.Barber, *Phys.Rev.A* **41**, 5187 (1990).
- [6] J.U.Nöckel, A.D.Stone and R.K.Chang, *Opt.Lett.***19**, 1693 (1994).
- [7] For an elementary treatment of KAM theory see L.E.Reichl, *The Transition to Chaos*, Springer-Verlag (1992). Although the term KAM theory is often used for the general theory of the transition to Hamiltonian chaos, in fact the KAM theorem does not apply to billiards due to the nonanalyticity of the “potential” at the boundary. The relevant theorem for smooth convex billiards is due to Lazutkin [8] but it leads to the same phenomenology as KAM.
- [8] V.F.Lazutkin, *Math.Izv.USSR* **37**, 186 (1973).
- [9] L.P.Kadanoff, *Phys.Rev.Lett.***47**, (1981).
- [10] J.B.Keller and S.I.Rubinow, *Ann.Phys.***9**, 24 (1960).
- [11] See M.V.Berry, *Eur.J.Phys.* **2** 91 (1981) for a good discussion.
- [12] J.U.Nöckel and A.D.Stone, unpublished.
- [13]  $\theta_{min}$  for a given shape  $\rho_b(z)$  is determined from the equation  $\tan \theta_{min} = L_z/z_m$  where  $z_m$  is the solution of  $\rho_b(z_m) = L_z$ .
- [14] See Ref.[11]; this statement is closely related to the well-known statement in resonator theory that spherical mirrors separated by less than twice their radius of curvature form “stable” resonators.